10

Dye-Sensitized Solar Cells Based on Polymer Electrolytes

Mi-Ra Kim, Sung-Hae Park, Ji-Un Kim and Jin-Kook Lee
Department of Polymer Science & Engineering, Pusan National University, Jangjeon-dong, Guemjeong-gu, Busan, South Korea

1. Introduction

Dye-sensitized solar cells (DSSCs) using organic liquid electrolytes have received significant attention because of their low production cost, simple structure and high power conversion efficiency [1-5]. Recently, the power conversion efficiencies of DSSCs using Ruthenium complex dyes, liquid electrolytes, and Pt counter electrode have reached 10.4 % (100 mW/cm^2, AM 1.5) by Grätzel group [6]. However, the important drawback of DSSCs using liquid electrolyte is the less long-term stability due to the volatility of the electrolyte contained organic solvent. In the viewpoint for commercialize, durability is a crucial component. Then, gel electrolytes are being investigated to substitute the liquid electrolytes [7-10]. One way to make a gel electrolyte is to add organic or inorganic (or both) materials. In the past decades, many studies have been carried out on this kind of gel electrolyte, and great progress has been achieved [11-12]. The advantages of them include; limited internal shorting, leakage of electrolytes and non-combustible reaction products at the electrode surface existing in the gel polymer electrolytes [13-14]. However, because of their complicated preparing technology and poor mechanical strength, they cannot be used in commercial production [15-16]. To overcome this problem, the polymer membrane is soaked in an electrolyte solution that has been examined [17-19].

To prepare the polymer membrane for polymer electrolyte, a number of processing techniques such as drawing [20], template synthesis [21-22], phase separation [23], electrospinning [24], etc. have been used. Among of these, the electrospinning technology is a simple and low-cost method for making ultra-thin diameter fibers. This technique, invented in 1934, makes use of an electrical field that is applied across a polymer solution and a collector, to force a polymer solution jet out from a small hole [25]. When the diameters of polymer fiber materials are shrunk of micrometers to submicrons or nanometers, several amazing characteristics appear such as a very large surface area to volume ratio, flexibility in surface functionalities, and superior mechanical performance compared to any other known forms of this material [26]. In recent years, the electrospinning method has gained greater attention. A vastly greater number of synthetic and natural polymer solutions were prepared with electrospun fibers, such as poly(ethylene oxide) (PEO) in distilled water [27], polyurethane in N,N-dimethylformamide (DMF) [28], poly(ε-caprolactone) (PCL) in acetone [29], PVDF in acetone/ N,N-dimethylacetamide (DMAc) (7:3 by weight) [30], and regenerated cellulose in 2:1(w/w) acetone/DMAc [31].

Many applications of electrospun fibers were also studied. In addition, this technique is highly versatile and allows the processing of not only many different polymers into polymeric nanofibers, but also the co-processing of polymer mixtures, mixtures of polymers, and low molecular weight nonvolatile materials, etc [13,32].

2. Principle

2.1 Dye-sensitized solar cells (DSSCs)

2.1.1 History of DSSCs

The history of the sensitization of semiconductors to light of wavelength longer than that corresponding to the band gap has been presented elsewhere [33,34]. It is an interesting convergence of photography and photo-electrochemistry, both of which rely on photo-induced charge separation at a liquid–solid interface. The silver halides used in photography have band gaps of the order of 2.7–3.2 eV, and are therefore insensitive to much of the visible spectrum, just as is the TiO_2 now used in these photo-electrochemical devices.

The material has many advantages for sensitized photochemistry and photo-electrochemistry: it is a low cost, widely available, non-toxic and biocompatible material, and as such is even used in health care products as well as domestic applications such as paint pigmentation. The standard dye at the time was *tris*(2,2′-bipyridyl-4,4′-carboxylate) ruthenium(II), the function of the carboxylate being the attachment by chemisorption of the chromophore to the oxide substrate. Progress thereafter, until the announcement in 1991 of the sensitized electrochemical photovoltaic device with a conversion efficiency at that time of 7.1% under solar illumination, was incremental, a synergy of structure, substrate roughness and morphology, dye photophysics [35] and electrolyte redox chemistry. That evolution has continued progressively since then, with certified efficiency now over 10%.

2.1.2 Structure and working principles of DSSCs

The DSSC consists of the following staffs (Fig. 1). (1) transparent conductive oxide glass (F-doped SnO_2 glass (FTO glass), (2) Nanoporous TiO_2 layers (diameter ; 15-20 nm), (3) dye monolayer bonded to TiO_2 nano-particles, (4) electrolytes consisting of I^- and I_3^- redox species, (5) platinum, (6) a counter electrode.

A schematic presentation of the operating principles of the DSSC is given in Fig. 2. At the heart of the system is a mesoscopic oxide semiconductor film, which is placed in contact with a redox electrolyte or an organic hole conductor. The choice of material has been TiO_2 (anatase) although alternative wide hand gap oxides such as ZnO, and Nb_2O_5 have also been investigated. Attached to the surface of the nanocrystalline film is a monolayer of the sensitizer. Photo-excitation of the latter results in the injection of an electron into the conduction band of the oxide. The dye is regenerated by electron donation from the electrolyte, usually an organic solvent containing a redox system, such as the iodide/ triiodide couple. The regeneration of the sensitizer by iodide intercepts the recapture of the reduction of the conduction band electron by the oxidized dye. The iodide is regenerated in turn by triiodide at the counter electrode when the circuit is completed via electron migration through the external load.

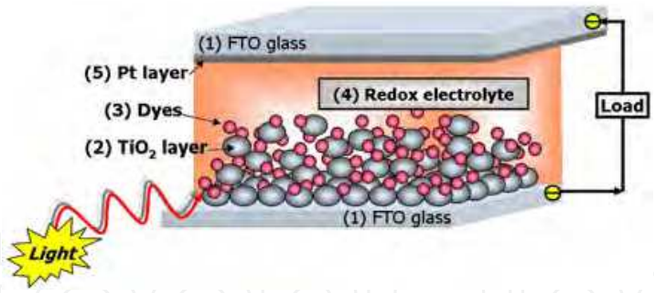

Fig. 1. A schematic presentation of a cross-section structure of the DSSC.

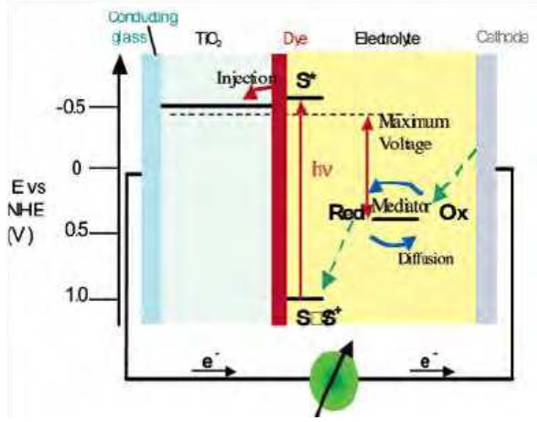

Fig. 2. A schematic presentation of the operating principles of the DSSC.

$$TiO_2/S + h\nu \rightarrow TiO_2/S^* \quad \text{(I)}$$

$$TiO_2/S^* \rightarrow TiO_2/S^+ + e_{cb} \quad \text{(II)}$$

$$TiO_2/S^+ + e_{cb} \rightarrow TiO_2/S \quad \text{(III)}$$

$$TiO_2/S^+ + (3/2)I^- \rightarrow TiO_2/S + (1/2)I_3^- \quad \text{(IV)}$$

$$(1/2)I_3^- + e_{(pt)} \rightarrow (3/2)I^-,\ I_3^- + 2e_{cb} \rightarrow 3I^- \quad \text{(V)}$$

Light absorption is performed by a monolayer of dye (S) adsorbed chemically at the semiconductor surface and excited by a photon of light (Eq. (I)). After having been excited (S*) by a photon of light, the dye-usually a transition metal complex whose molecular properties are specifically for the task is able to transfer an electron to the semiconductor (TiO_2) by the injection process (Eq. (II)). The efficiency of a DSSC in the process for energy conversion depends on the relative energy levels and the kinetics of electron transfer processes at the liquid junction of the sensitized semiconductor/electrolyte interface. For efficient operation of the cell, the rate of electron injection must be faster than the decay of the dye excited state. Also, the rate of rereduction of the oxidized dye (dye cation) by the electron donor in the electrolyte (Eq. (IV)) must be higher than the rate of back reaction of the injected electrons with the dye cation (Eq. (III)), as well as the rate of reaction of injected electrons with the electron acceptor in the electrolyte (Eq. (V)). Finally, the kinetics of the reaction at the counter electrode must also guarantee the fast regeneration of charge mediator (Eq. (V)), or this reaction could also become rate limiting in the overall cell performance [36-39].

2.1.3 Present DSSC research and development

2.1.3.1 Sensitizer (Dye)

The ideal sensitizer for a single junction photovoltaic cell converting standard global AM 1.5 sunlight to electricity should absorb all light below a threshold wavelength of about 920 nm. In addition, it must also carry attachment groups such as carboxylate or phosphonate to firmly graft it to the semiconductor oxide surface. Upon excitation it should inject electrons into the solid with a quantum yield of unity. The energy level of the excited state should be well matched to the lower bound of the conduction band of the oxide to minimize energetic losses during the electron transfer reaction.
Its redox potential should be sufficiently high that it can be regenerated via electron donation from the redox electrolyte or the hole conductor. Finally, it should be stable enough to sustain about 108 turnover cycles corresponding to about 20 years of exposure to natural light.

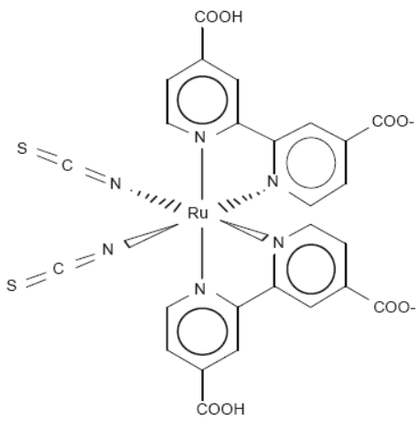

Fig. 3. Chemical structure of the N3 ruthenium complex used as a charge transfer sensitizer in DSSCs.

The best photovoltaic performance both in terms of conversion yield and long-term stability has so far been achieved with polypyridyl complexes of ruthenium and osmium. Sensitizers having the general structure $ML_2(X)_2$, where L stands for 2,2′-bipyridyl-4,4′-dicarboxylic acid M is Ru or Os and X presents a halide, cyanide, thiocyanate, acetyl acetonate, thiacarbamate or water substituent, are particularly promising. Thus, the ruthenium complex *cis*-$RuL_2(NCS)_2$, known as N3 dye, shown in Fig. 3 has become the paradigm of heterogeneous charge transfer sensitizer for mesoporous solar cells.

2.1.3.2 Mesoporous oxide film development

When the dye-sensitized nanocrystalline solar cell was first presented, perhaps the most puzzling phenomenon was the highly efficient charge transport through the nanocrystalline TiO_2 layer. The mesoporous electrodes are very much different compared to their compact analogs because (i) the inherent conductivity of the film is very low; (ii) the small size of the nanocrystalline particles does not support a built-in electrical field; and (iii) the electrolyte penetrates the porous film all the way to the back-contact making the semiconductor/electrolyte interface essentially three-dimensional. Charge transport in mesoporous systems is under keen debate today and several interpretations based on the Montrol Scher model for random displacement of charge carriers in disordered solids [40]

have been advanced. However, the "effective" electron diffusion coefficient is expected to depend on a number of factors such as trap filling and space charge compensation by ionic motion in the electrolyte. Therefore, the theoretical and experimental effort will continue as there is a need for further in depth analysis of this intriguing charge percolation process. The factors controlling the rate of charge carriers percolation across the nanocrystalline film are presently under intense scrutiny. Intensity modulated impedance spectroscopy has proved to be an elegant and powerful tool [41,42] to address important questions related to the characteristic time constants for charge carrier transport and reaction dynamics in DSSCs. On the material science side, future research will be directed towards synthesizing structures with a higher degree of order than the random fractal-like assembly of nanoparticles shown in Fig. 4. A desirable morphology of the films would have the mesoporous channels or nanorods aligned in parallel to each other and vertically with respect to the transparent conducting oxide (TCO) glass current collector. This would facilitate pore diffusion, give easier access to the film surface avid grain boundaries and allow the junction to be formed under better control.

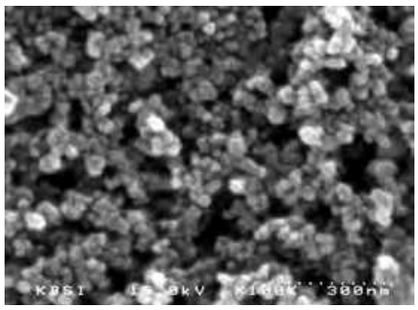

Fig. 4. Scanning electron micrograph of a sintered mesoscopic TiO_2 film supported on an FTO glass. The average particle size is 20 nm.

One approach to fabricate such oxide structures is based on surfactant templates assisted preparation of TiO_2 nanotubes as described in recent paper by Adachi et al. [43]. The hybrid nanorod-polymer composite cells developed by Huynh et al. [44] have confirmed the superior photovoltaic performance of such films with regards to random particle networks.

2.1.3.3 Polymer electrolytes

The polymer-based material is generally produced in a thin-film configuration by casting or spin-coating techniques. Polymer electrolytes are composed by alkaline salts (e.g. lithium or sodium salts) dissolved in a high molar mass polyether host (e.g. poly(ethylene oxide) (PEO) or poly(propylene oxide) (PPO)) [45]. In polymer electrolytes, the polymer matrix should be an efficient solvent for the salt, capable of dissociating it and minimizing the formation of ion pairs. The solubility of the salt relies on the ability of the electron donor atoms in the polymer chain to coordinate the cation through a Lewis type acid–base interaction. This interaction also depends on the lattice energy of the salt and the structure of the host polymer. The mechanism for ionic motion in polymer electrolytes results from a solvation–desolvation process along the chains that occurs predominantly in the amorphous polymer phase. Since the ionic motion is strictly correlated with the segmental motion of the polymer chains, the ionic conductivity increases with increasing chain mobility. The ionic conductivity is also a function of the number of charge carriers in the polymer matrix. However, above a limiting high salt concentration the segmental motion of the polymer chains is reduced due to an "ionic cross-linking" which decreases ionic conductivity [46].

2.1.4 Characteristics of DSSCs

There are several factors for characterization of DSSCs below; (See Fig. 5).

2.1.4.1 Incident photon-to current efficiency (IPCE)

The Incident Photon-to-Current Efficiency (IPCE), also called external quantum efficiency, is defined as the number of electrons generated by light in the external circuit divided by the number of incident photons as a function of excitation wavelength. It is expressed in Eq. (1) [47]. A high IPCE is a prerequisite for high-power photovoltaic applications, which depends on the sensitizer photon absorption, excited state electron injection. And electrons transport to the terminals.

$$IPCE = [(1.25x10^{3}) \times \text{photocurrent density}(mAcm^{-2})] \times [\text{Wavelength}(nm) \times \text{photon flux}\ (Wm^{-2})\ ]^{-1} \quad (1)$$

2.1.4.2 Open-circuit voltage (V_{oc})

If there is no external circuit, the incoming photons will still create hole-electron pairs and they will still travel downhill to the layers, but they will pile up there because there is no external wire. The number of carriers leaking back is equal to the number being generated by the incoming light, an equilibrium voltage has been reached. This is called the open-circuit voltage (V_{oc}). In DSSCs, V_{oc} is defined by the difference between Fermi level of TiO_2 and redox potential of electrolyte [10].

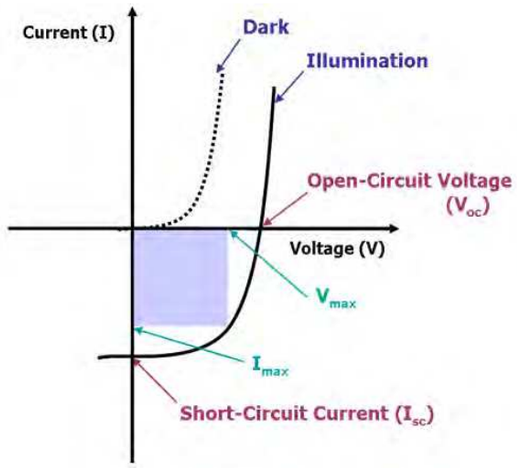

Fig. 5. Several factors for characterization of DSSC.

2.1.4.3 Short-circuit current (I_{sc}) and Short-circuit current density (J_{sc})

If the external circuit is simply a wire and has no appreciable resistance, the current that flows is the short-circuit current (I_{sc}) and is directly related to the number of photons of light being absorbed by the cell. Short-circuit current density (J_{sc}) is short-circuit current per active area.

2.1.4.4 Fill factor (FF)

The fill factor (FF) is obtained by diving the product of current and voltage measured at the power point (maximum output power P_{max}) by the product of short-circuit current and the open-circuit voltage. The power point is the maximum product of the cell voltage and the photocurrent obtained on the I-V curve.

$$P_{max} = I_{max} \times V_{max} = FF \times I_{sc} \times V_{oc} \quad (2)$$

$$FF = P_{max} / I_{sc} \times V_{oc} \quad (3)$$

2.1.4.5 Power conversion efficiency

The power conversion efficiency (η) of the dye-sensitized solar cell is determined by the photocurrent density measured at short-circuit, V_{oc}, the FF of the cell, and the intensity of the incident light (P_i) as shown in follow equation.

$$\eta = I_{sc} \times V_{oc} \times FF / P_i \quad (4)$$

Sometimes the use of the ratio of the maximum power output (P_{max}) to the incident power input (P_{in}), defined as

$$\eta = P_{max} / P_{in} = I_{sc} \times V_{oc} \times FF / P_{in} \quad (5)$$

2.1.5 Advantages and disadvantages of DSSCs

The major advantage of the concept of dye sensitization is the fact that the conduction mechanism is based on a majority carrier transport as opposed to the minority carrier transport of conventional inorganic cells. This means that bulk or surface recombination of the charge carriers in the TiO_2 semiconductor cannot happen. Thus, impure starting materials and a simple cell processing without any clean room steps are permitted, yet resulting in promising power conversion efficiencies of 7 - 11% and the hope of a low-cost device for photoelectrochemical solar energy conversion. On the other hand impure materials can result in a strongly reduced lifetime of the cells. The most important issue of the dye-sensitized cells is the stability over the time and the temperature range which occurs under outdoor conditions. Although it could be shown, that intrinsic degradation can considerably be reduced, the behavior of the liquid electrolyte under extreme conditions is still unknown. For a successful commercialization of these cells, the encapsulation/sealing, the coloration and the electrolyte filling has to be transferred into fully automated lines including the final closure of the filling openings. Therefore, a significant effort is taken in order to replace the liquid electrolyte by a gel electrolyte, a solid-state electrolyte or a p-type conducting polymer material.

2.2 Electrospinning

2.2.1 History of electrospinning method

The process of using electrostatic forces to form synthetic fibers, known as electrospinning, has been known for over 100 years. From 1934 to 1944, Formhals published a series of patents [25,48,49,50], describing an experimental setup for the production of polymer filaments using an electrostatic force. A polymer solution, such as cellulose acetate, was introduced into the electric field. It was not until 1934, when Formhals patented a process, that electrospinning truly surfaced as a valid technique for sinning small-diameter fibers. In 1952, Vonnegut and Neubauer were able to produce streams of highly electrified uniform droplets of about 0.1mm in diameter [51]. They invented a simple apparatus for the electrical atomization. In 1955, Drozin investigated the dispersion of a series of liquids into aerosols under high electric potentials [52]. Formhals studied for a better understanding of the electrospinning process; however, it would be nearly 30years before Taylor would publish work regarding the jet forming process. In 1969, Taylor published his work examining how the polymer droplet at the end of a capillary behaves when an electric field is applied [53]. In his studies he found that the pendant droplet develops into a cone (now

called the Taylor cone) when the surface tension is balanced by electrostatic forces. In 1971, Baumgarten made an apparatus to electrospun acrylic fibers with diameters in the range of 0.05-1.1 microns [54]. Since 1980s and especially in recent years, the electrospinning process has regained more attention probably due to interest in nanotechnology, as ultrafine fibers or fibrous structures of various polymers with diameters down to submicrons or nanometers can be easily fabricated with this process. One of the most important applications of traditional micro-size fibers, especially engineering fibers such and carbon, glass, and Kevlar fivers is to be used as reinforcements in composite developments [55]. In addition to composite reinforcement, other application fields based on electrospun polymer nanofibers, such as medical prosthesis [55-57], filtration, cosmetics [59], tissue engineering [60], liquid crystal device [61], electromagnetic shielding and photovoltaic device [62], have been steadily extended especially in recent years.

2.2.2 Principles of electrospinning method

Fig. 6 shows the schematic diagram of the electrospinning method. There are basically three components to fulfill this process: a high voltage supplier, a capillary tube with a pipette or needle of a small diameter, and a metal collecting screen. A typical electrospinning setup consists of a capillary through which the liquid to be electrospun is forced; a high voltage source with positive or negative polarity, which injects charge into the liquid; and a grounded collector. Once it has been ejected out of the metal needle with a small hole, the polymer solution was introduced into the electric field. The polymer filaments formed between two electrodes bearing electrical charges of opposite polarity. Before the polymer solution reach the collector, the polymer solution jet evaporates or solidifies, and is collected as an interconnecting web of small fibers. One of these electrodes was placed into the solution and the other onto a collector (Fig. 7).

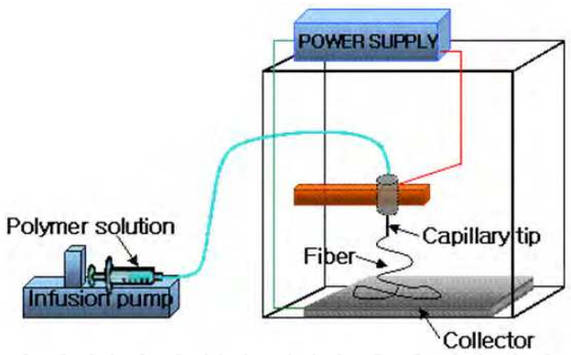

Fig. 6. Schematic diagram of the electrospinning method.

2.2.3 Ideal targets of electrospun nanofibers

As long as a polymer can be electrospun into nanofibers, ideal targets would be in that: (1) the diameters of the fibers be consistent and controllable, (2) the fiber surface be defect-free or defect-controllable, and (3) continuous single nanofibers be collectable. However researches so far have shown that there three targets are by no means easily achievable [26].

2.2.4 Processing parameters

There are a number of processing parameters that can greatly affect fiber formation and structure. The parameters are polymer concentration, applied voltage, flow rate, tip to

collector distance (TCD) and Solvent volatility. Furthermore, all parameters can influence the formation of bead defects.

2.2.4.1 Polymer concentration

The polymer concentration determines the spinnability of a solution, namely whether a fiber forms or not. The solution must have a high enough polymer concentration for chain entanglements to occur; however the solution cannot be either too dilute or too concentrated. If the solution is too dilute then the fibers break up into droplets before reaching the collector due to the effects of surface tension. However, if the solution is too concentrated then fibers cannot be formed due to the high viscosity, which makes it difficult to control the solution flow rate through the capillary. Thus, an optimum range of polymer concentrations exists in which fibers can be electrospun when all other parameters are held constant. A higher viscosity results in a larger fibers diameter [53, 63]. When polymers dissolve in a solvent, the solution viscosity is proportional to the polymer concentration. Thus, the higher the polymer concentration the larger the resulting nanofiber diameters will be.

2.2.4.2 Applied voltage

The strength of the applied electric field controls formation of fibers from several microns in diameter to tens of nanometers. Deitzel et al. examined a polyethylene oxide (PEO)/water system and found that increases in applied voltage altered the shape of the surface at which the Taylor cone and fiber jet were formed [64]. At lower applied voltages the Taylor cone formed at the tip of the drop; however, as the applied voltage was increased the volume of the drop decreased until the Taylor cone was formed at the tip of the capillary, which was associated with an increase in bead defects seen among the electrospun fibers (Fig.8). Moreover, another parameter which affects the fiber diameter to a remarkable extent is the applied voltage. In general, a higher applied voltage ejects more fluid in a jet, resulting in a larger fiber diameter [27].

2.2.4.3 Flow rate

Polymer flow rate also has an impact of fiber size, and additionally can influence fiber porosity as well as fiber shape. In the Taylor's work, they realized that the cone shape at the tip of the capillary cannot be maintained if the flow of solution through the capillary is insufficient to replace the solution ejected as the fiber jet [53]. They demonstrated that both fiber diameter and pore size increase with increasing flow rate. Additionally, at high flow rates significant amounts of bead defects were noticeable, due to the inability of fibers to dry completely before reaching the collector [60].

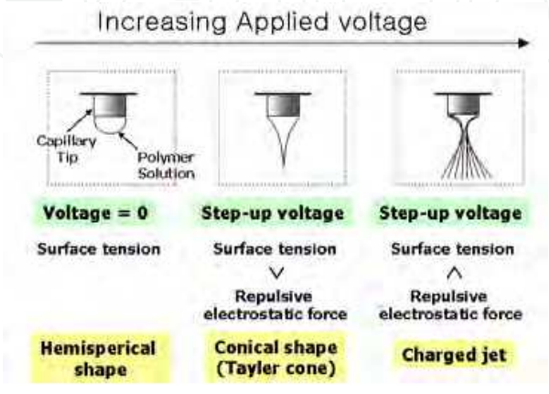

Fig. 7. Effect of varying the applied voltage on the formation of the Taylor cone.

2.2.4.4 Tip to collector distance (TCD)

The distance of between capillary tip and collector can also influence fiber size by 1-2 orders of magnitude. Additionally, this distance can dictate whether the end result is electrospinning or electrospraying. Doshi and Reneker found that the fiber diameter decreased with increasing distances from the Taylor cone [65].

2.2.4.5 Solvent volatility

Choice of solvent is also critical as to whether fibers are capable of forming, as well as influencing fiber porosity. In order for sufficient solvent evaporation to occur between the capillary tip and the collector a volatile solvent must be used. As the fiber jet travels through the atmosphere toward the collector a phase separation occurs before the solid polymer fibers are deposited, a process that is greatly influenced by volatility of the solvent. Zhao et al. examined the structural properties of 15 wt % of poly(Vinylidene Fluoride) nanofibers with different volume ratios in DMF/Acetone [66]. When DMF was used as the solvent without acetone, bead-fibers were found. When 9:1 DMF/acetone was used a s the solvent in the polymer solution, beads in the electrospun almost disappeared. Furthermore, the ultafine fibers without beads demonstrated clearly when the acetone amount in the solution increased to 20 %. Acetone is more volatile than DMF. Furthermore, the changes of solution properties by the addition of acetone could probably improve the electrospun membrane morphology and decrease the possibility of bead formation.

3. Results

3.1 Preparation of electrospun poly(vinylidene fluoride-hexafluoropropylene) (PVDF-HFP) nanofibers

Generally, in the electrospinning method, the changing of the parameters had a great effect on fiber morphology. To prepare the electrospun PVDF-HFP nanofiber films with the suitable morphology, we prepared the electrospun PVDF-HFP nanofiber films by several parameters such as the applied voltage(voltage supplier: NNC-ESP100, Nano NC Co., Ltd.), the tip-to-collector distance (TCD), and the concentration of the PVDF-HFP. First, the PVDF-HFP was dissolved in acetone/DMAc (7/3 weight ratio) for 24 hours at room temperature. Then, we prepared the electrospun PVDF-HFP nanofibers by the electrospinning method with different parameters. The applied voltage was ranged from 8 to 14 kV, TCD was varied from 13 to 21 cm, and the concentration of PVDF-HFP varied from 11 to 17 wt %. On all occasions, we used a syringe pump (781100, Kd Scientific) to control the flow rate of the polymer solution, the solution flow rate was 2 ml/h.

In the electrospinning method, the changing of the polymer concentration had a great effect on fiber morphology. To investigate the influence of polymer concentrations on the electrospun PVDF-HFP nanofibers, we prepared the PVDF-HFP nanofibers. When the polymer concentration were varied from 11 wt% to 17 wt%, TCD and applied voltages were 15 cm and 14 kV, respectively. Over the polymer solution of 19 wt% and below the polymer solution of 9 wt%, the nanofibers did not form. Fig. 8 shows the surface images of the electrospun PVDF-HFP nanofibers observed by FE-SEM and the diameter distributions of nanofibers. The increase of the polymer concentration resulted in an increase of the average fiber diameter of the electrospun PVDF-HFP nanofibers. In particular, the PVDF-HFP nanofiber, which was prepared from 15 wt% of polymer concentration showed a highly regular morphology with an average diameter of 800 - 1000 nm.

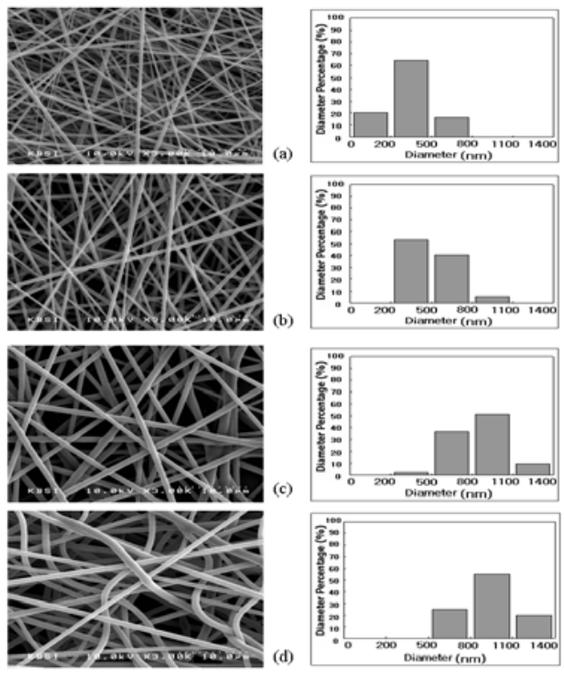

Fig. 8. FE-SEM images of electrospun PVDF-HFP nanofibers with different polymer concentrations (Applied voltage = 14 kV, TCD = 15 cm, flow rate = 2 ml/h) and their diameter distributions: (a) 11 wt%, (b) 13 wt%, (c) 15 wt%, (d) 17 wt%.

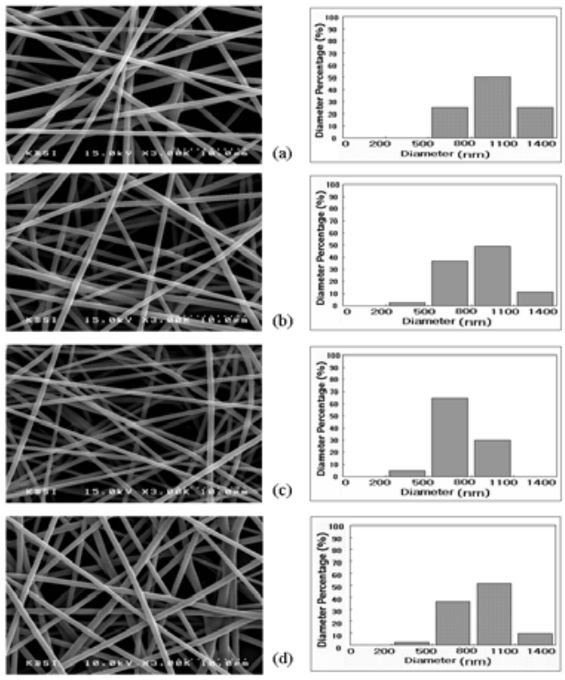

Fig. 9. FE-SEM images of electrospun PVDF-HFP nanofiber with different applied voltages (TCD = 15 cm, polymer concentration = 15 wt%, flow rate = 2 ml/h) and their diameter distributions: (a) 8 kV, (b) 10 kV, (c) 12 kV, (d) 14 kV.

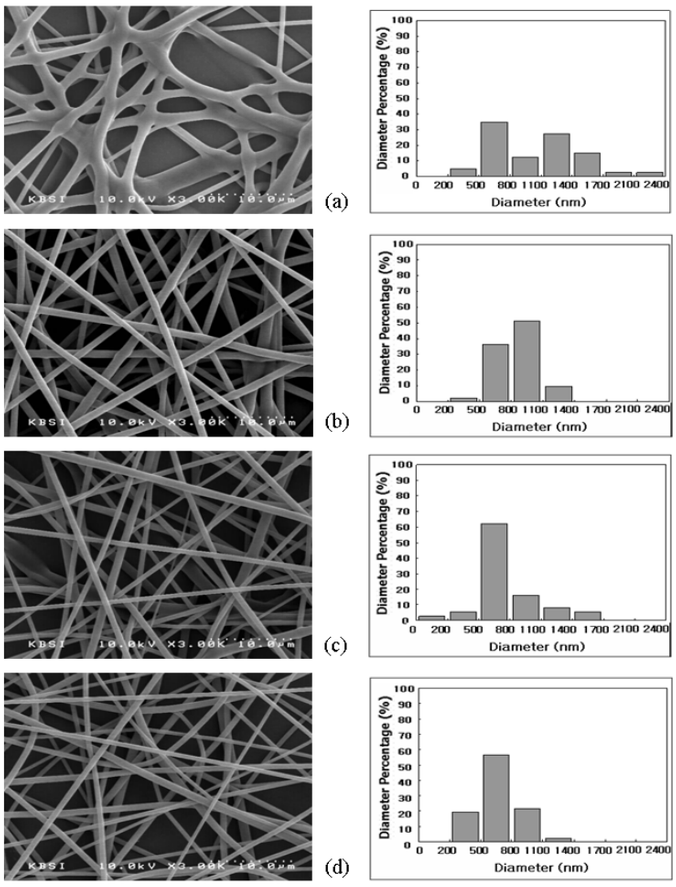

Fig. 10. FE-SEM images of electrospun PVDF-HFP nanofibers with different TCDs (Applied voltage = 14 kV, polymer concentration = 15 wt%, flow rate = 2 ml/h) and their diameter distributions: (a) 13 cm, (b) 15 cm, (c) 17 cm, (d) 19 cm.

To investigate the effect of applied voltage, experiments were carried out when the applied voltage was varied from 8 kV to 14 kV, TCD and polymer concentrations were held at 15 cm and 15 wt%, respectively. The morphologies of electrospun PVDF-HFP nanofibers prepared are shown in Fig. 9.

In addition, we prepared the electrospun PVDF-HFP nanofibers when the TCD was varied from 13 cm to 19 cm, applied voltage and polymer concentrations were held at 14 kV and 15 wt%, respectively. The morphologies of prepared electrospun PVDF-HFP nanofibers prepared are shown in Fig. 10. When the TCD was just close below 13 cm, irregular fiber morphology was formed, because the polymer jet arrived at the collector before the solidification. Therefore, we were able to optimize the preparation condition at an applied voltage of 14 kV, a polymer concentration of 15 wt%, and TCD of 15 cm to obtain the regular PVDF-HFP nanofibers.

As the changing of such parameters in the electrospinning method, the diameter and the morphology of the nanofibers fabricated were changed. At the condition of the 15 wt% of PVDF-HFP polymer solution, 14 kV of the applied voltage, 15 cm of the TCD and 2 ml/h of the flow rate, the nanofibers of the electrospun PVDF-HFP films showed extremely regular morphology with diameter of average 0.8 ~ 1.0 μm.

3.2 Characterizations of PVDF-HFP nanofibers

The pore size, the volume fraction and interconnectivity of pore domain, and the type of porous polymer matrix will determine the uptake and the ion conductivity of the electrolyte [63]. To investigate the effect of porous polymer matrix, the spin-coated PVDF-HFP film was also fabricated by using conventional spin-coating method, and measured the ionic conductivity under the same condition. The ionic conductivity of the spin-coated PVDF-HFP film was 1.37×10^{-3} S/cm, and this value showed lower value than the electrospun PVDF-HFP nanofiber film.

To measure the uptake and the porosity of the electropsun PVDF-HFP nanofiber films from electrolyte solution, the electropsun PVDF-HFP nanofiber films were taken out from the electrolyte solution after activation and excess electrolyte solution on the film surface was wiped.

The electrolyte uptake (U) was evaluated according to the following formula:

$$U = [(m-m_0)/m_0]\times100\%$$

where m and m_0 are the masses of wet and dry of the electrospun nanofiber films, respectively.

The porosity (P) of the electrospun nanofibers was calculated from the density of electrospun PVDF-HFP nanofibers (ρ_m, g/cm^3) and the density of pure PVDF-HFP (ρ_p= 1.77g/cm^3):

$$P\ (\text{vol.}\%) = (1-\rho_m/\rho_p)\times100$$

The density of the electrospun PVDF-HFP nanofibers was determined by measuring the volume and the weight of the electrospun PVDF-HFP nanofibers. The uptake and the porosity of the electrospun PVDF-HFP nanofiber film was obtained 653±50 % and 70±2.3 %, respectively, regardless the diameter and the morphology of nanofibers prepared with various parameters.

3.3 Fabrications of DSSCs devices using PVDF-HFP nanofibers

We prepared the DSSC devices, sandwiched with working electrode using TiO_2 impregnated dyes and counter electrode using a platinum (Pt, T/SP) electrode as two electrodes. The DSSC device was fabricated using this following process. The TiO_2 pastes (Ti-Nanoxide, HT/SP) were spread on a FTO glass using the doctor blade method and calcinated at 500 ^oC. The sensitizer *Cis*-di(thiocyanato)-N,N-bis(2,2'-bypyridil-4.4'-dicarboxylic acid)ruthenium (II) complex (N3 dye) was dissolved in pure ethanol in a concentration of 20 mg per 100 ml of solution. The FTO glass deposited TiO_2 was dipped in an ethanol solution at 45 ^oC for 18 hours. The electospun PVDF-HFP nanofibers or the spin-coated PVDF-HFP film were cut by 0.65 cm × 0.65 cm after drying, and put on the TiO_2 adsorbed the dyes, the electrolyte solution was dropped above them, and dried in a dry oven at 45 ^oC for 2 hours to evaporate wholly the solvent. To compare with the electrospun PVDF-HFP nanofiber films, the conventional spin-coating method was used for making a spin-coated PVDF-HFP film. In all cases, the thickness of the electrospun PVDF-HFP nanofibers and spin-coated PVDF-HFP film were 30±1 μm by using digimatic micrometer. The electrolyte was consisted of 0.10 M of iodine (I_2), 0.30 M of 1-propyl-3-methylimidazolium iodide (PMII), and 0.20 M of tetrabutylammonium iodide (TBAI) in the solution of ethylene carbonate (EC)/ propylene carbonate (PC)/ acetonitrile (AN) (8:2:5

v/v/v). The Pt pastes were spread on a FTO glass using the doctor blade method and calcinated at 400 °C.

3.4 Photovoltaic properties of the DSSC devices using PVDF-HFP nanofibers

The DSSC devices using several different electrospun PVDF-HFP nanofibers on various parameters were fabricated and their photovoltaic characteristics are summarized in Table 1 – 3. I-V curves of the DSSC devices using them are shown in Fig. 11. The concentration of the PVDF-HFP solution was 15 wt% in acetone/DMAc (7/3 by weight ratio). The photovoltaic characteristics of the DSSC devices were measured by using Solar Simulator (150 W simulator, PEC-L11, PECCELL) under AM 1.5 and 100 mW/cm² of the light intensity.

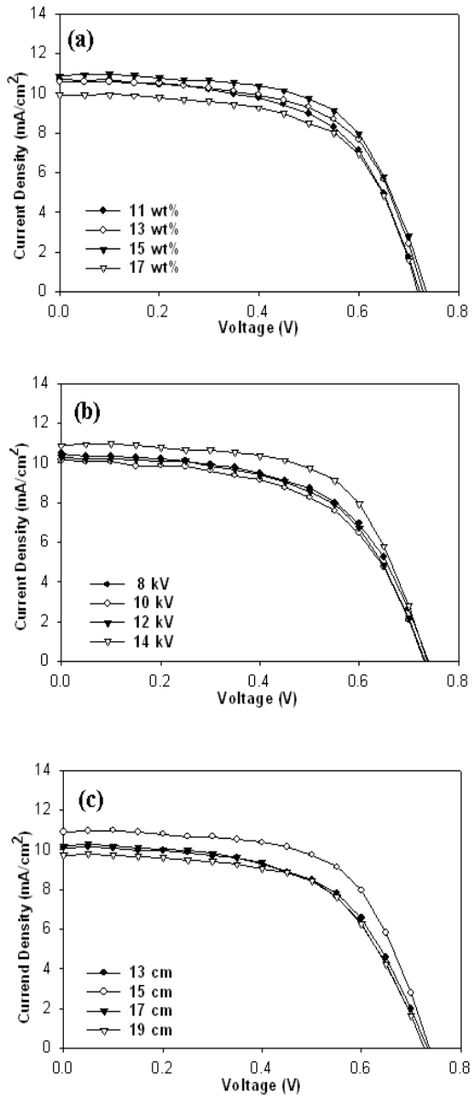

Fig. 11. I-V curves of DSSC devices using electrospun PVDF-HFP nanofibers under illumination at AM 1.5 condition: (a) different polymer concentrations, (b) different applied voltages, (c) different TCDs.

Polymer concentration (wt.%)	V_{OC} (V)	J_{SC} (mA/cm²)	FF	η (%)
11	0.74	10.88	0.60	4.78
13	0.73	10.57	0.62	4.78
15	0.74	10.89	0.63	5.02
17	0.72	9.92	0.62	4.41

Table 1. Photovoltaic performances of DSSC devices using electrospun PVDF-HFP nanofibers on different polymer concentrations

Applied voltage (kV)	V_{OC} (V)	J_{SC} (mA/cm²)	FF	η (%)
8	0.74	10.50	0.57	4.41
10	0.73	10.10	0.56	4.17
12	0.74	10.30	0.58	4.35
14	0.74	10.88	0.63	5.02

Table 2. Photovoltaic performances of DSSC devices using electrospun PVDF-HFP nanofibers on different applied voltages

TCD (cm)	V_{OC} (V)	J_{SC} (mA/cm²)	FF	η (%)
13	0.73	10.10	0.58	4.30
15	0.74	10.88	0.63	5.02
17	0.73	10.20	0.57	4.23
19	0.73	9.72	0.60	4.21

Table 3. Photovoltaic performances of DSSC devices using electrospun PVDF-HFP nanofibers on different TCDs

Type	V_{OC} (V)	J_{SC} (mA/cm²)	FF	η (%)
Electrospun PVDF-HFP nanofiber film	0.75	12.3	0.57	5.21
Spin-coated PVDF-HFP film	0.67	3.87	0.55	1.43

Table 4. Photovoltaic characteristics of DSSC devices using electrospun PVDF-HFP nanofiber film and spin-coated PVDF-HFP film in polymer electrolytes

The active area of the DSSC devices measured by using a black mask was 0.25 cm². The V_{OC}, J_{SC}, FF, and η of the DSSC device using the spin-coated PVDF-HFP film were 0.67 V, 3.87 mA/cm², 0.56, and 1.43 %, respectively. The η of DSSC device using the spin-coated PVDF-HFP film was lower than it of the DSSC device using electrospun PVDF-HFP nanofiber films, because of the decrease of J_{SC}, and all data are summarized in Table 4 and their I-V curves are shown in Fig. 12. This result seemed that because the porosity of the electrospun PVDF-HFP nanofibers is higher than it of the spin-coated PVDF-HFP film, ion transfer occurred well and regular nanofiber morphology helped to transfer ion produced by redox

mechanism, therefore, overall power conversion efficiency of DSSC devices using the electrospun PVDF-HFP nanofiber films was higher than that of the DSSC device using spin-coated PVDF-HFP film. However, the minute change of nanofibers diameter was influenced little on power conversion efficiency.

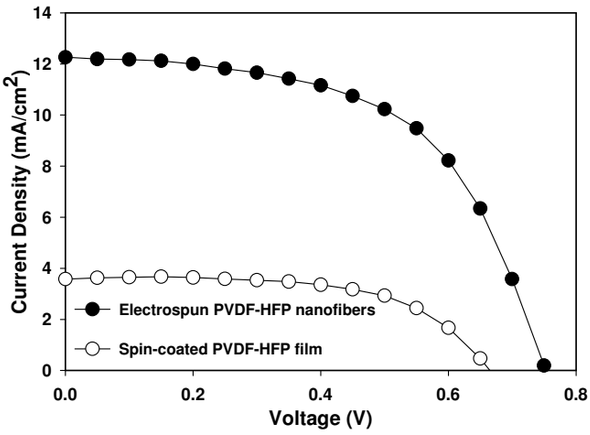

Fig. 12. I-V curves of the DSSC devices using electrospun PVDF-HFP nanofibers and spin-coated PVDF-HFP film.

3.5 Effect of electrolyte in the electrospun PVDF-HFP nanofibers on DSSC

The photovoltaic performance of DSSC devices using the electrospun PVDF-HFP nanofibers showed remarkable improved results compared to DSSC devices using the spin-coated PVDF-HFP film. To prove these results, the interfacial charge transfer resistances were investigated by the EIS measurement. The EIS data were measured with impedance analyzer at same condition using FTO/TiO_2/electrolyte/Pt/FTO cells, and fitted by Z-MAN software (WONATECH) and Echem analyst (GAMRY). The Nyquist plots of the FTO/TiO_2/electrolyte/Pt/FTO cells and charge transfer resistances are shown in Fig. 13 and Table 5, respectively. The equivalent circuit of DSSC devices is shown in Fig. 14. The R_S, $R1_{CT}$ and $R2_{CT}$ were series resistance, the charge transfer resistance of Pt/electrolyte interface, and the charge transfer resistance of TiO_2/electrolyte interface, respectively. The $R2_{CT}$ of the DSSC device using the spin-coated PVDF-HFP film was similar to that of the DSSC device using the electrospun PVDF-HFP nanofibers. However, the R_S and $R1_{CT}$ of the DSSC device using the spin-coated PVDF-HFP film were higher than those of the DSSC device using the electrospun PVDF-HFP nanofibers. These results showed that the spin-coated film has a higher resistance than the electropun nanofibers, and poor I^-/I^{3-} activity between Pt and electrolyte affected to the low value of the J_{SC}. As a result, the η of the DSSC device using the spin-coated PVDF-HFP film showed low value.

Type	R_S (Ω)	$R1_{CT}$ (Ω)	$R2_{CT}$ (Ω)
Electrospun PVDF-HFP nanofibers	21.70	11.01	11.07
Spin-coated PVDF-HFP film	31.87	25.02	14.37

Table 5. The series resistances (R_S), the charge transfer resistance of the Pt/electrolyte ($R1_{CT}$) and TiO_2/electrolyte ($R2_{CT}$) in the DSSC devices under AM 1.5 by the EIS measurement

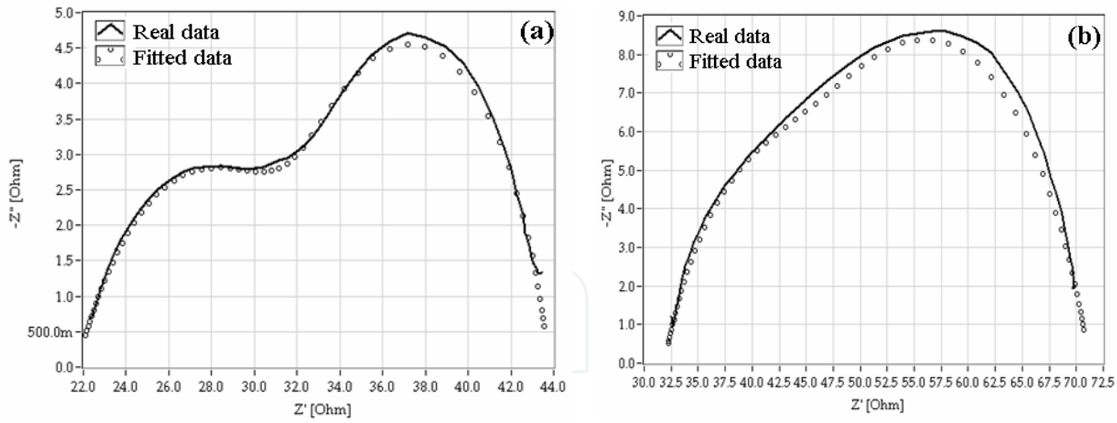

Fig. 13. Nyquist plots the FTO/TiO_2/electrolyte/Pt/FTO device using (a) electrospun PVDF-HFP nanofiber film electrolyte, and (b) spin-coated PVDF-HFP film electrolyte.

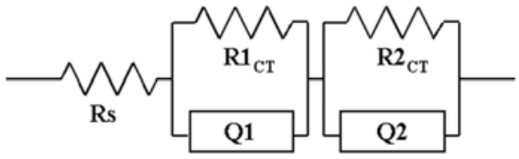

Fig. 14. The equivalent circuit of the DSSC device. (R_S: Series resistance, $R1_{CT}$: charge transfer resistance of Pt/electrolyte, $R2_{CT}$: charge transfer resistance of TiO_2/electrolyte, Q1 and Q2: constant phase element)

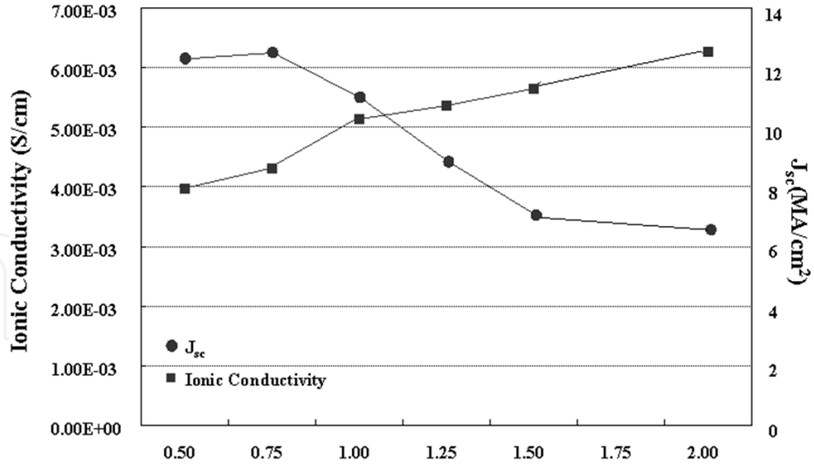

Fig. 15. Ionic conductivities of electrospun PVDF-HFP nanofiber films and J_{sc} of DSSC devices using electrospun PVDF-HFP nanofiber films with mole ratio of iodine to TBAI.

In addition, to investigate the photovoltaic effect of I_2 concentrations on DSSC using the electrospun PVDF-HFP nanofiber, we prepared FTO/TiO_2/Dye/Electrolyte/Pt/FTO devices with various mole ratios of I_2 to TBAI in electrolyte solutions. In Table 6, as the increase of the I_2 concentration in electrolyte, the ionic conductivity of the electrospun

PVDF-HFP nanofiber films increased, while the photocurrent density of the DSSC devices using the electrospun PVDF-HFP nanofibers electrolyte decreased. The relationship between the ionic conductivity the electrospun PVDF-HFP nanofiber films and the photocurrent density of the DSSC devices are illustrated in Fig. 15 and I-V curves are shown in Fig. 16. In general, the photocurrent density of DSSC using the liquid electrolyte is proportionate to the ionic conductivity in electrolyte. From these results, we found that the photocurrent density and the efficiency on DSSC using the electrospun PVDF-HFP nanofibers electrolyte are not necessarily proportionate to the ionic conductivity in electrolyte.

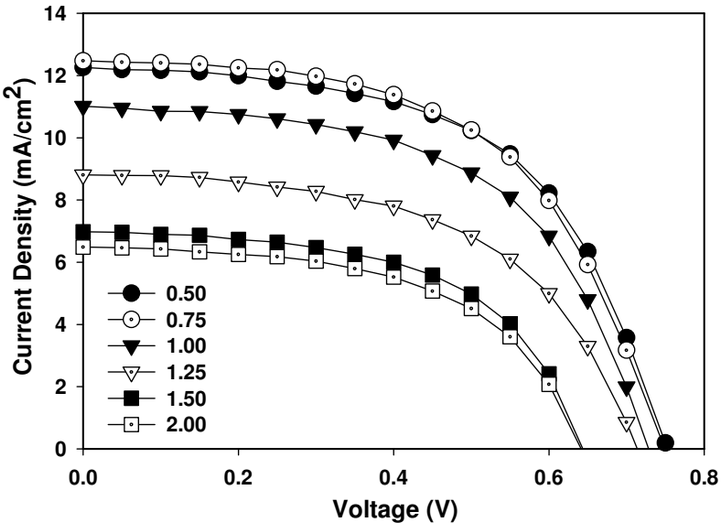

Fig. 16. The I-V curves of the DSSC devices using electrospun PVDF-HFP nanofibers with mole ratio of iodine to TBAI.

4. Future outlooks

During the rebirth of polymer electrospining over the past decade the applicability of electrospun fibers has become apparent across many fields. This highly adaptable process allows the formation of functional fibrous membranes for applications such as tissue engineering, drug delivery, sensor, cosmetic and photovoltaic devices. Electrospun nanofibers offer an unprecedented flexibility and modularity in design. Improvements in strength and durability, and their incorporation in composite membranes, will allow there scaffolds to compete with existing membrane technology. Currently, the research field of electrospnning is ripe with functional materials from resorbable cells to ceramic solid-phase catalyst and continued research interest is expected to improve most areas of full cells and photovoltaic cells.

5. Acknowledgement

This research was supported by the Converging Research Center Program through the National Research Foundation of Korea (NRF) funded by the Ministry of Education, Science and Technology (20090082141).

6. References

Adachi, M.; Murata, Y.; Okada, I. & Yoshikawa, S. (2003). Formation of Titania Nanotubes and Applications for Dye-Sensitized Solar Cells. *Journal of the Electrochemical Society*, Vol. 150, No. 8, pp. G488-G493, ISSN 0013-4651

Amadelli, R.; Argazzi, R.; Bignozzi, C. A. & Scandola, F. (1990). Design of antenna-sensitizer polynuclear complexes. Sensitization of titanium dioxide with [Ru(bpy)2(CN)2]2Ru(bpy(COO)2)22. *Journal of the American Chemical Society*, Vol. 112, No. 20, pp. 7099-7103, ISSN 0002-7863

Anton, Formhals (1934). Process and apparatus for preparing artificial threads. US Patent 1,975,504.

Anton, Formhals (1939). Method and apparatus for spinning. US Patent 2160962

Anton, Formhals (1940). Artificial thread and method of producing same. US Patent 2187306

Anton, Formhals (1944). Method and apparatus for spinning. US Patent 2349950

Armand, M. (1990). Polymers with Ionic Conductivity. *Advanced Materials*, Vol. 2, No. 6-7, pp. 278-286, ISSN 1521-4095

Asano, T.; Kubo, T. & Nishikitani, Y. (2004). Electrochemical properties of dye-sensitized solar cells fabricated with PVDF-type polymeric solid electrolytes. *Journal of Photochemistry and Photobiology A: Chemistry*, Vol. 164, No. 1-3, pp. 111-115, ISSN 1010-6030

Bach, U.; Lupo, D.; Comte, P.; Moser, J. E.; Weissortel, F.; Salbeck, J.; Spreitzer, H. & Gratzel, M. (1998). Solid-state dye-sensitized mesoporous TiO2 solar cells with high photon-to-electron conversion efficiencies. *Nature*, Vol. 395, No. 6702, pp. 583-585, ISSN 0028-0836

Baumgarten, P. K. (1971). Electrostatic spinning of acrylic microfibers. *Journal of Colloid and Interface Science*, Vol. 36, No. 1, pp. 71-79, ISSN 0021-9797

Berry, John P. (Wirral, GB2) (1990). Electrostatically produced structures and methods of manufacturing. US Patent 4965110

Bornat, A. L., GB2) (1987). Production of electrostatically spun products. US Patent 4689186

Cao, J. H.; Zhu, B. K. & Xu, Y. Y. (2006). Structure and ionic conductivity of porous polymer electrolytes based on PVDF-HFP copolymer membranes. *Journal of Membrane Science*, Vol. 281, No. 1-2, pp. 446-453, ISSN 0376-7388

Caruso, R. A.; Schattka, J. H. & Greiner, A. (2001). Titanium Dioxide Tubes from Sol–Gel Coating of Electrospun Polymer Fibers. *Advanced Materials*, Vol. 13, No. 20, pp. 1577-1579, ISSN 1521-4095.

Chand, S. (2000). Review Carbon fibers for composites. *Journal of Materials Science*, Vol. 35, No. 6, pp. 1303-1313, ISSN 0022-2461

Deitzel, J. M.; Kleinmeyer, J.; Harris, D. & Tan, N. C. B. (2001). The effect of processing variables on the morphology of electrospun nanofibers and textiles. *Polymer*, Vol. 42, No. 1, pp. 261-272, ISSN 0032-3861

Deitzel, J. M.; Kleinmeyer, J.; Harris, D. & Tan, N. C. B. (2001). The effect of processing variables on the morphology of electrospun nanofibers and textiles. *Polymer*, Vol. 42, No. 1, pp. 261-272, ISSN 0032-3861.

Demir, M. M.; Yilgor, I.; Yilgor, E. & Erman, B. (2002). Electrospinning of polyurethane fibers. *Polymer*, Vol. 43, No. 11, pp. 3303-3309, ISSN 0032-3861

Dloczik, L.; Ileperuma, O.; Lauermann, I.; Peter, L. M.; Ponomarev, E. A.; Redmond, G.; Shaw, N. J. & Uhlendorf, I. (1997). Dynamic Response of Dye-Sensitized Nanocrystalline Solar Cells: Characterization by Intensity-Modulated Photocurrent

Spectroscopy. *The Journal of Physical Chemistry B*, Vol. 101, No. 49, pp. 10281-10289, ISSN 1520-6106

Doshi, J. & Reneker, D. H. (1995). Electrospinning process and applications of electrospun fibers. *Journal of Electrostatics*, Vol. 35, No. 2-3, pp. 151-160, ISSN 0304-3886

Drozin, V. G. (1955). The electrical dispersion of liquids as aerosols. *Journal of Colloid Science*, Vol. 10, No. 2, pp. 158-164, ISSN 0095-8522

Feng, L.; Li, S.; Li, H.; Zhai, J.; Song, Y.; Jiang, L. & Zhu, D. (2002). Super-Hydrophobic Surface of Aligned Polyacrylonitrile Nanofibers. *Angewandte Chemie International Edition*, Vol. 41, No. 7, pp. 1221-1223, ISSN 1521-3773

Grätzel, M. (2004). Conversion of sunlight to electric power by nanocrystalline dye-sensitized solar cells. *Journal of Photochemistry and Photobiology A: Chemistry*, Vol. 164, No. 1-3, pp. 3-14, ISSN 1010-6030

Hagfeldt, A. & Gratzel, M. (1995). Light-Induced Redox Reactions in Nanocrystalline Systems. *Chemical Reviews*, Vol. 95, No. 1, pp. 49-68, ISSN 0009-2665

Hagfeldt, A. & Grätzel, M. (2000). Molecular Photovoltaics. *Accounts of Chemical Research*, Vol. 33, No. 5, pp. 269-277, ISSN 0001-4842

Hohman, M. M.; Shin, M.; Rutledge, G. & Brenner, M. P. (2001). Electrospinning and electrically forced jets. II. Applications. *Physics of Fluids*, Vol. 13, No. 8, pp. 2221-2236, ISSN 1070-6631

Hou, H. Q.; Jun, Z.; Reuning, A.; Schaper, A.; Wendorff, J. H. & Greiner, A. (2002). Poly(p-xylylene) nanotubes by coating and removal of ultrathin polymer template fibers. *Macromolecules*, Vol. 35, No. 7, pp. 2429-2431, ISSN 0024-9297

Hu Y. J.; Chen B.; Yuan Y. (2007). Preparation and Electrochemical Properties of Polymer Li-ion Battery Reinforced by non-woven Fabric. *J. Cent. South Univ.Technol, Vol. 14, No. 1*, pp. 47-49, ISSN 1005-9784

Huang, H. T. & Wunder, S. L. (2001). Ionic conductivity of microporous PVDF-HFP/PS polymer blends. *Journal of the Electrochemical Society*, Vol. 148, No. 3, pp. A279-A283, ISSN 0013-4651

Huang, Z.-M.; Zhang, Y. Z.; Kotaki, M. & Ramakrishna, S. (2003). A review on polymer nanofibers by electrospinning and their applications in nanocomposites. *Composites Science and Technology*, Vol. 63, No. 15, pp. 2223-2253, ISSN 0266-3538

Huynh, W. U.; Dittmer, J. J. & Alivisatos, A. P. (2002). Hybrid Nanorod-Polymer Solar Cells. *Science*, Vol. 295, No. 5564, pp. 2425-2427, ISSN 0036-8075

Jeong, Y.-B. & Kim, D.-W. (2004). Cycling performances of Li/LiCoO2 cell with polymer-coated separator. *Electrochimica Acta*, Vol. 50, No. 2-3, pp. 323-326, ISSN 0013-4686

Kalyanasundaram, K. & Grätzel, M. (1998). Applications of functionalized transition metal complexes in photonic and optoelectronic devices. *Coordination Chemistry Reviews*, Vol. 177, No. 1, pp. 347-414, ISSN 0010-8545

Kelly, C. A. & Meyer, G. J. (2001). Excited state processes at sensitized nanocrystalline thin film semiconductor interfaces. *Coordination Chemistry Reviews*, Vol. 211, No. 1, pp. 295-315, ISSN 0010-8545

Kim, D. W. & Sun, Y. K. (2001). Electrochemical characterization of gel polymer electrolytes prepared with porous membranes. *Journal of Power Sources*, Vol. 102, No. 1-2, pp. 41-45, ISSN 0378-7753

Kim, D. W.; Kim, Y. R.; Park, J. K. & Moon, S. I. (1998). Electrical properties of the plasticized polymer electrolytes based on acrylonitrile-methyl methacrylate copolymers. *Solid State Ionics*, Vol. 106, No. 3-4, pp. 329-337, ISSN 0167-2738

Kim, J. R.; Choi, S. W.; Jo, S. M.; Lee, W. S. & Kim, B. C. (2005). Characterization and properties of P(VdF-HFP)-based fibrous polymer electrolyte membrane prepared

by electrospinning. *Journal of the Electrochemical Society*, Vol. 152, No. 2, pp. A295-A300, ISSN 0013-4651

Komiya, R.; Han, L.; Yamanaka, R.; Islam, A. & Mitate, T. (2004). Highly efficient quasi-solid state dye-sensitized solar cell with ion conducting polymer electrolyte. *Journal of Photochemistry and Photobiology A: Chemistry*, Vol. 164, No. 1-3, pp. 123-127, ISSN 1010-6030

Liu, H. & Hsieh, Y.-L. (2003). Surface methacrylation and graft copolymerization of ultrafine cellulose fibers. *Journal of Polymer Science Part B: Polymer Physics*, Vol. 41, No. 9, pp. 953-964, ISSN 1099-0488

M. Armand, in: J.R. MacCallum, C.A. Vincent (Eds.). (1987). Current state of PEO-based electrolyte *Polymer Electrolyte Reviews-1*, Elsevier Applied Science, London

Ma P. X.; Zhang R. (1999). *Synthetic nano-scale fibrous extracellular matrix*. pp. 60-72, John Wiley

Martin, C. R. (1996). Membrane-Based Synthesis of Nanomaterials. *Chemistry of Materials*, Vol. 8, No. 8, pp. 1739-1746, ISSN 0897-4756

McEvoy, A. J. & Grätzel, M. (1994). Sensitisation in photochemistry and photovoltaics. *Solar Energy Materials and Solar Cells*, Vol. 32, No. 3, pp. 221-227, ISSN 0927-0248

Meyer, G. J. (1997). Efficient Light-to-Electrical Energy Conversion: Nanocrystalline TiO2 Films Modified with Inorganic Sensitizers. *Journal of Chemical Education*, Vol. 74, No. 6, pp. 652l, ISSN 0021-9584

Michot, T.; Nishimoto, A. & Watanabe, M. (2000). Electrochemical properties of polymer gel electrolytes based on poly(vinylidene fluoride) copolymer and homopolymer. *Electrochimica Acta*, Vol. 45, No. 8-9, pp. 1347-1360, ISSN 0013-4686

Nazeeruddin, M. K.; Kay, A.; Rodicio, I.; Humphry-Baker, R.; Mueller, E.; Liska, P.; Vlachopoulos, N. & Graetzel, M. (1993). Conversion of light to electricity by cis-X2bis(2,2'-bipyridyl-4,4'-dicarboxylate)ruthenium(II) charge-transfer sensitizers (X = Cl-, Br-, I-, CN-, and SCN-) on nanocrystalline titanium dioxide electrodes. *Journal of the American Chemical Society*, Vol. 115, No. 14, pp. 6382-6390, ISSN 0002-7863

Nelson, J. (1999). Continuous-time random-walk model of electron transport in nanocrystalline TiO_{2} electrodes. *Physical Review B*, Vol. 59, No. 23, pp. 15374, ISSN 1098-0121

Nogueira, A. F. & De Paoli, M.-A. (2000). A dye sensitized TiO2 photovoltaic cell constructed with an elastomeric electrolyte. *Solar Energy Materials and Solar Cells*, Vol. 61, No. 2, pp. 135-141, ISSN 0927-0248

Ondarçuhu, T. & Joachim, C. (1998). Drawing a single nanofibre over hundreds of microns. *EPL (Europhysics Letters)*, Vol. 42, No. 2, pp. 215, ISSN 0295-5075

O'Regan, B. and M. Gratzel (1991). A low-cost, high-efficiency solar cell based on dye-sensitized colloidal TiO2 films. *Nature*, Vol.353, No.6346, pp. 737-740, ISSN 0028-0836

Péchy, P.; Renouard, T.; Zakeeruddin, S. M.; Humphry-Baker, R.; Comte, P.; Liska, P.; Cevey, L.; Costa, E.; Shklover, V.; Spiccia, L.; Deacon, G. B.; Bignozzi, C. A. & Grätzel, M. (2001). Engineering of Efficient Panchromatic Sensitizers for Nanocrystalline TiO2-Based Solar Cells. *Journal of the American Chemical Society*, Vol. 123, No. 8, pp. 1613-1624, ISSN 0002-7863

Reneker, D. H.; Kataphinan, W.; Theron, A.; Zussman, E. & Yarin, A. L. (2002). Nanofiber garlands of polycaprolactone by electrospinning. *Polymer*, Vol. 43, No. 25, pp. 6785-6794, ISSN 0032-3861

Senecal, Kris (N. Smithfield, RI, US); Samuelson, Lynne (Marlborough, MA, US); Sennett, Michael (Sudbury, MA, US); Schreuder-gibson, Heidi (Holliston, MA, US) (2006). Conductive (electrical, ionic, and photoelectric) polymer membrane articles, and method for producing same. US Patent 7109136

Sill, T. J. & von Recum, H. A. (2008). Electrospinning: Applications in drug delivery and tissue engineering. *Biomaterials*, Vol. 29, No. 13, pp. 1989-2006, ISSN 0142-9612

Smith, Daniel J. (Stow, OH); Reneker, Darrell H. (Akron, OH); Mcmanus, Albert T. (San Antonio, TX); Schreuder-gibson, Heidi L. (Holliston, MA); Mello, Charlene (Rochester, MA); Sennett, Michael S. (Sudbury, MA) (2004). Electrospun fibers and an apparatus therefor. US Patent 6753454

Stephan, A. M.; Nahm, K. S.; Anbu Kulandainathan, M.; Ravi, G. & Wilson, J. (2006). Poly(vinylidene fluoride-hexafluoropropylene) (PVdF-HFP) based composite electrolytes for lithium batteries. *European Polymer Journal*, Vol. 42, No. 8, pp. 1728-1734, ISSN 0014-3057

Stergiopoulos, T.; Arabatzis, I. M.; Katsaros, G. & Falaras, P. (2002). Binary Polyethylene Oxide/Titania Solid-State Redox Electrolyte for Highly Efficient Nanocrystalline TiO2 Photoelectrochemical Cells. *Nano Letters*, Vol. 2, No. 11, pp. 1259-1261, ISSN 1530-6984

Sze S M. (1981). *Physics of Semiconductor Devices* (New York : Wiley) p 264

Taylor, G. (1969). Electrically Driven Jets. *Proceedings of the Royal Society of London. Series A, Mathematical and Physical Sciences*, Vol. 313, No. 1515, pp. 453-475, ISSN 0080-4630

van de Lagemaat, J.; Park, N. G. & Frank, A. J. (2000). Influence of Electrical Potential Distribution, Charge Transport, and Recombination on the Photopotential and Photocurrent Conversion Efficiency of Dye-Sensitized Nanocrystalline TiO2 Solar Cells: A Study by Electrical Impedance and Optical Modulation Techniques. *The Journal of Physical Chemistry B*, Vol. 104, No. 9, pp. 2044-2052, ISSN 1520-6106

Vonnegut, B. & Neubauer, R. L. (1952). Production of monodisperse liquid particles by electrical atomization. *Journal of Colloid Science*, Vol. 7, No. 6, pp. 616-622, ISSN 0095-8522

Wang, P.; Zakeeruddin, S. M. & Grätzel, M. (2004). Solidifying liquid electrolytes with fluorine polymer and silica nanoparticles for quasi-solid dye-sensitized solar cells. *Journal of Fluorine Chemistry*, Vol. 125, No. 8, pp. 1241-1245, ISSN 0022-1139

Wang, P.; Zakeeruddin, S. M.; Moser, J. E.; Nazeeruddin, M. K.; Sekiguchi, T. & Gratzel, M. (2003). A stable quasi-solid-state dye-sensitized solar cell with an amphiphilic ruthenium sensitizer and polymer gel electrolyte. *Nat Mater*, Vol. 2, No. 6, pp. 402-407, ISSN 1476-1122

Watanabe, M.; Kanba, M.; Matsuda, H.; Tsunemi, K.; Mizoguchi, K.; Tsuchida, E. & Shinohara, I. (1981). High lithium ionic conductivity of polymeric solid electrolytes. *Die Makromolekulare Chemie, Rapid Communications*, Vol. 2, No. 12, pp. 741-744, ISSN 0173-2803

Waters, Colin M. (Tattingstone, GB2); Noakes, Timothy J. (Selbourne, GB2); Pavey, Ian (Fernhurst, GB2); Hitomi, Chiyoji (Tsokuba, JP) (1992). Liquid crystal devices. US Patent 5088807

Zhizhen Zhao, Jingquing Li, Xiaoyan Yuan Xing Li, Yuanyuan Zhang, Jing Sheng. (2005). *journal of Applied Polmer Scence, 97*, 466-474. Zhao, Z. Z.; Li, J. Q.; Yuan, X. Y.; Li, X.; Zhang, Y. Y. & Sheng, J. (2005). Preparation and properties of electrospun poly(vinylidene fluoride) membranes. *Journal of Applied Polymer Science*, Vol. 97, No. 2, pp. 466-474, ISSN 0021-8995

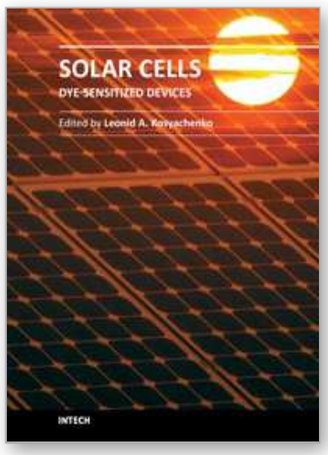

Solar Cells - Dye-Sensitized Devices
Edited by Prof. Leonid A. Kosyachenko

ISBN 978-953-307-735-2
Hard cover, 492 pages
Publisher InTech
Published online 09, November, 2011
Published in print edition November, 2011

The second book of the four-volume edition of "Solar cells" is devoted to dye-sensitized solar cells (DSSCs), which are considered to be extremely promising because they are made of low-cost materials with simple inexpensive manufacturing procedures and can be engineered into flexible sheets. DSSCs are emerged as a truly new class of energy conversion devices, which are representatives of the third generation solar technology. Mechanism of conversion of solar energy into electricity in these devices is quite peculiar. The achieved energy conversion efficiency in DSSCs is low, however, it has improved quickly in the last years. It is believed that DSSCs are still at the start of their development stage and will take a worthy place in the large-scale production for the future.

INTECH
open science | open minds

InTech Europe
University Campus STeP Ri
Slavka Krautzeka 83/A
51000 Rijeka, Croatia
Phone: +385 (51) 770 447
Fax: +385 (51) 686 166
www.intechopen.com

InTech China
Unit 405, Office Block, Hotel Equatorial Shanghai
No.65, Yan An Road (West), Shanghai, 200040, China
中国上海市延安西路65号上海国际贵都大饭店办公楼405单元
Phone: +86-21-62489820
Fax: +86-21-62489821

IntechOpen